

Free Vibration analysis of Curvilinearly Stiffened Composite plates with an arbitrarily shaped cutout using Isogeometric Analysis

Balakrishnan Devarajan^{a,*}

^a*Department of Biomedical Engineering and Mechanics, Virginia Polytechnic Institute and State University, Blacksburg, VA 24061, USA*

Abstract

This paper focuses on the isogeometric vibration analysis of curvilinearly stiffened composite panels. The stiffness matrices and the mass matrices are derived using the first-order shear deformation theory (FSDT). The present method models the plate and the stiffener separately, which allows the stiffener element nodes to not coincide with the plate shell-element nodes. The stiffness and mass matrices of a stiffener are transformed to those of the plate through the displacement compatibility conditions at the plate–stiffener interface via the novel mapping technique. Cutouts are modeled using a single NURBS patch generated by creating a ruled surface between two curves. The proposed formulation is first validated by comparing it with available literature. The effects of width-to-thickness ratio, fiber orientation, ply layups, shape and size of the cutouts and the boundary conditions on the response of stiffened composite plates are then analyzed and the numerical results are used to derive useful conclusions.

Keywords: Isogeometric analysis, NURBS, Free vibration, Buckling, Composite laminates, curvilinear stiffeners, stiffened panels, Cutouts, Structural Mechanics

*Corresponding Author

Email address: dbalak9@vt.edu (Balakrishnan Devarajan)

1. Introduction

Due to their exceptional specific stiffness-to-weight and strength-to-weight ratios, composite materials are witnessing increased utilization in aircraft structures [1]. Recent strides in manufacturing techniques, exemplified by the NASA Integrated Structural Assembly of Advanced Composites (ISSAC) robot and the creation of unitized stiffened composite panels through vacuum assisted resin transfer molding, have enabled the construction of intricate composite structures in atypical aircraft configurations, leading to lighter and more eco-friendly designs. These innovative manufacturing processes necessitate the development of efficient analysis and design tools tailored for stiffened composite panels produced using such methods.

The incorporation of curvilinear stiffeners, spars, or ribs in aircraft design introduces an expanded design domain, notably benefiting wing designs through heightened structural performance and reduced overall weight [2, 3, 4, 5, 6, 7, 8, 9, 10, 11, 12]. This is due to the flexibility they offer in terms of geometric curvature in addition to the placement and orientation.

In practice, many aerospace structures encounter unpredictable pressure loads, making determinism impractical. Vibrations stemming from gust loads, engine noise, and auxiliary electrical systems can also generate noise within aircraft. Consequently, all flight vehicles function within a realm of random vibration. A comprehensive examination of finite element free vibration and dynamic analysis for composite laminated plates was presented by Zhang and Yang [13]. Reddy and Khdeir [14] explored buckling and vibration responses in composite laminated plates, employing a variety of plate theories including classical, first, and third-order laminate theories. Carrera et al. [15] scrutinized the vibration of slender composite plates under various in-plane loads, utilizing Carrera's unified formulation and finite element techniques.

Stiffened composite structures have found extensive application across engineering contexts, enhancing vibration response while concurrently reducing panel weight. Lee and Lee [16] delved into the effects of fiber ply orientation, dimensions, and stiffener placement on free vibration modes of anisotropic stiffened plates, employing the first-order shear deformation theory. Rikards et al. [17] adopted an equivalent layer shell theory to examine buckling and vibration responses in laminated composite stiffened shells. Patel et al. [18] investigated the static and dynamic instability traits of stiffened shells subjected to uniform in-plane harmonic edge loading using finite element

methodologies. Mukherjee and Mukhopadhyay [19] employed isoparametric shell elements to conduct vibrational analysis on plates with eccentric stiffeners. The displacement and geometry of the stiffeners were related to those of the plates using the displacement compatibility condition, which utilizes interpolation functions in the finite element method. Kumar and Mukhopadhyay [20] employed a beam element to represent the stiffener within a stiffened laminated plate. The displacement and geometry of the stiffener's beam element nodes were interpolated based on the nodes of the plate's shell element at the location of the stiffener's beam element node. Subsequently, this model was adopted by multiple researchers for both stiffened isotropic plates/shells and stiffened laminated plates in analyses involving buckling [20], vibration [21], thermal effects, free vibration, and transient dynamic behavior [22].

Isogeometric Analysis (IGA) was introduced by Hughes et al. [23, 24] which implements an isoparametric formulation by using NURBS basis functions to describe the geometry and to construct the finite basis approximations. The IGA developed rapidly and has been successfully applied in various fields [25, 26, 27, 28, 29] including laminated composite plates [30, 31, 32] and functionally graded plates under a thermal environment [33, 34, 35]. Even though Qin et al. [36] used IGA isogeometric analysis to analyze the static response of stiffened panels, studies emphasizing isogeometric analysis for the vibrational behavior of stiffened composite plates are limited.

Due to an increase in requirement of laminated composite for a plethora of engineering applications, the use of plates with arbitrarily shaped cutouts are unavoidable. The response of structures to loads can be significantly affected due to the presence of cutouts. Since the study of laminated composites with cutouts is a complex problem, numerical methods are used extensively. Vibration and buckling analysis of such structures have been performed using various numerical approaches like the finite strip method [37], the finite element method (FEM) [38, 39, 40], meshfree methods [41], Rayleigh — Ritz method [42] and [43], extended finite element method (XFEM) [44]. Isogeometric analysis [23, 45] is being widely used over the last ten years. It offers many benefits such as exact geometry representation, easy mesh refinement, higher-order continuity, and it avoids the mesh generation procedure when using the traditional way. Many insights into splines techniques [46], mathematical properties [47, 48] and integration method [49, 50] have been gained. Many problems have been successfully solved using IGA including fluid mechanics [47], plates and shells [51, 52, 31, 30] damage and fracture mechanics

[53], contact mechanics [54] and structural shape optimization [55]. Based on the best knowledge of the authors, no such identical task has been examined when this manuscript is being reported. The first section takes the readers through the mathematical formulation of the plate and the stiffener followed by the modeling technique used for generating arbitrary shaped cutouts. The final section discusses the results and the advantages of the present method over some existing methods.

2. Mathematical Foundation

In the first-order shear deformation theory (FSDT) the displacement field is considered as the first-order Taylor expansion of mid-plane variables with respect to plate thickness as follows: Consider a stiffened composite panel as shown in Figure 1. The mid-plane of the panel O_{xy} the global coordinate system. The plate is assumed to have a uniform thickness with no plydrops. Let u be the displacements in the x -axis and v be the in-plane displacements along the y -axis. Let w be the transverse deflection along the z -axis.

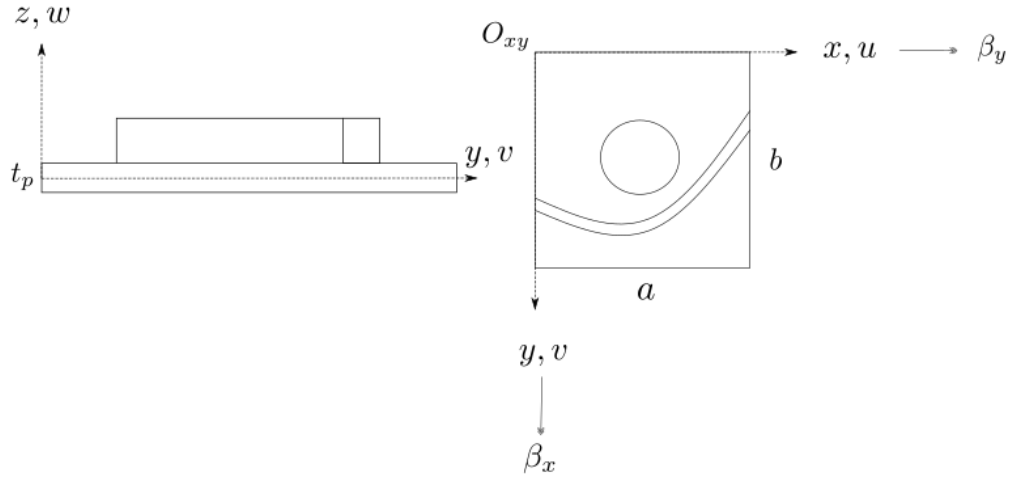


Figure 1: Geometry and nomenclature of a stiffened composite panel with a central cutout. Redrawn and modified from [56]

Let β_y and β_x be rotation components of the panel around the x - and y -axes, respectively. The displacement components of the panel is defined by

the first-order shear-deformable theory as follows,

$$\begin{aligned} u(x, y, z, t) &= u_0(x, y, z, t) + z\beta_x(x, y, t) \\ v(x, y, z, t) &= v_0(x, y, z, t) + z\beta_y(x, y, t) \\ w(x, y, z, t) &= w_0(x, y, z, t) \end{aligned} \quad (1)$$

The plate strain energy U_p can be written as,

$$U_p = \frac{1}{2} \int_{\Omega} \int_{\Omega} \boldsymbol{\varepsilon}_p^{\text{LT}} \mathbf{D}_p \boldsymbol{\varepsilon}_p^{\text{L}} d\Omega \quad (2)$$

Where, \mathbf{D}_p depends on the material property, stacking sequence, ply orientation and thickness of the plate. Derivation of \mathbf{D}_p is explained in Section 2.1. The generalized strains $\boldsymbol{\varepsilon}_p$ and the generalized displacements \mathbf{u}_p of the panel can be written as,

$$\boldsymbol{\varepsilon}_p^{\text{L}} = \begin{Bmatrix} \varepsilon_x^0 \\ \varepsilon_y^0 \\ \gamma_{xy}^0 \\ \kappa_x^0 \\ \kappa_y^0 \\ \kappa_{xy}^0 \\ \gamma_{xz}^0 \\ \gamma_{yz}^0 \end{Bmatrix} = \begin{bmatrix} \frac{\partial}{\partial x} & 0 & 0 & 0 & 0 & 0 \\ 0 & \frac{\partial}{\partial x} & 0 & 0 & 0 & 0 \\ \frac{\partial}{\partial x} & \frac{\partial}{\partial x} & 0 & 0 & 0 & 0 \\ 0 & 0 & 0 & 0 & \frac{\partial}{\partial x} & 0 \\ 0 & 0 & 0 & 0 & 0 & \frac{\partial}{\partial x} \\ 0 & 0 & 0 & 0 & \frac{\partial}{\partial x} & \frac{\partial}{\partial x} \\ 0 & 0 & 0 & \frac{\partial}{\partial x} & 1 & 0 \\ 0 & 0 & 0 & \frac{\partial}{\partial x} & 0 & 1 \end{bmatrix} \begin{Bmatrix} u_0 \\ v_0 \\ w_0 \\ \beta_x \\ \beta_y \end{Bmatrix} = \mathbf{B}_p \mathbf{u}_p \quad (3)$$

The panel strain energy U_p for the composite panel is,

$$U_p = \frac{1}{2} \iint_{\Omega} \mathbf{u}_p^T \mathbf{B}_p^T \mathbf{D}_p \mathbf{B}_p \mathbf{u}_p d\Omega \quad (4)$$

The kinetic energy T_p for the composite panel is,

$$T_p = \frac{1}{2} \iint_{\Omega} \dot{\mathbf{u}}_p^T m_p \dot{\mathbf{u}}_p d\Omega \quad (5)$$

Where,

$$\mathbf{m}_p = \rho \begin{pmatrix} t & 0 & 0 & 0 & 0 \\ 0 & t & 0 & 0 & 0 \\ 0 & 0 & t & 0 & 0 \\ 0 & 0 & 0 & t^2/12 & 0 \\ 0 & 0 & 0 & 0 & t^2/12 \end{pmatrix} \quad (6)$$

2.1. Orthotropic layers

The constitutive equation in the local coordinate system for the k^{th} orthotropic elastic laminate can be derived from Hooke's law as

$$\begin{Bmatrix} \sigma_1 \\ \sigma_2 \\ \tau_{12} \\ \sigma_3 \\ \tau_{31} \\ \tau_{23} \end{Bmatrix}^{(k)} = \begin{bmatrix} Q_{11} & Q_{12} & 0 & 0 & 0 & 0 \\ Q_{21} & Q_{22} & 0 & 0 & 0 & 0 \\ 0 & 0 & Q_{66} & 0 & 0 & 0 \\ Q_{31} & Q_{32} & 0 & Q_{33} & 0 & 0 \\ 0 & 0 & 0 & 0 & Q_{55} & 0 \\ 0 & 0 & 0 & 0 & 0 & Q_{44} \end{bmatrix}^{(k)} \begin{Bmatrix} \varepsilon_1 - \alpha_1 \Delta T \\ \varepsilon_2 - \alpha_2 \Delta T \\ \gamma_{12} \\ \varepsilon_3 - \alpha_3 \Delta T \\ \gamma_{31} \\ \gamma_{23} \end{Bmatrix}^{(k)} \quad (7)$$

where Q_{ij} are the elastic coefficients in the material coordinate system, T is the temperature change and α_i is the thermal coefficient of expansion in the principal i^{th} -direction. The transformed material constants are expressed as,

$$\begin{Bmatrix} \overline{Q}_{11} \\ \overline{Q}_{12} \\ \overline{Q}_{22} \\ \overline{Q}_{16} \\ \overline{Q}_{26} \\ \overline{Q}_{66} \end{Bmatrix} = \begin{bmatrix} c^4 & 2c^2s^2 & s^4 & 4c^2s^2 \\ c^2s^2 & c^4 + s^4 & c^2s^2 & -4c^2s^2 \\ s^4 & 2c^2s^2 & c^4 & 4c^2s^2 \\ c^3s & cs(s^2 - c^2) & -cs^3 & 2cs(s^2 - c^2) \\ cs^3 & cs(c^2 - s^2) & -c^3s & 2cs(c^2 - s^2) \\ c^2s^2 & -2c^2s^2 & c^2s^2 & (c^2 - s^2)^2 \end{bmatrix} \begin{Bmatrix} Q_{11} \\ Q_{12} \\ Q_{22} \\ Q_{66} \end{Bmatrix}, \quad (8)$$

$$\begin{bmatrix} \overline{Q}_{44} & \overline{Q}_{13} \\ \overline{Q}_{45} & -\overline{Q}_{36} \\ \overline{Q}_{55} & \overline{Q}_{23} \end{bmatrix} = \begin{bmatrix} c^2 & s^2 \\ -cs & cs \\ s^2 & c^2 \end{bmatrix} \begin{bmatrix} Q_{44} & Q_{13} \\ Q_{55} & Q_{23} \end{bmatrix}, \quad \overline{Q}_{33} = Q_{33} \quad (9)$$

$$\begin{Bmatrix} \alpha_x \\ \alpha_y \\ \alpha_{xy} \end{Bmatrix} = \begin{bmatrix} c^2 & s^2 \\ s^2 & c^2 \\ 2cs & -2cs \end{bmatrix} \begin{Bmatrix} \alpha_1 \\ \alpha_2 \end{Bmatrix}, \quad \alpha_z = \alpha_3 \quad (10)$$

where $c = \cos \theta$ and $s = \sin \theta$.

Using this, \mathbf{D}_p can now be written as

$$\mathbf{D}_p = \begin{bmatrix} \mathbf{A} & \mathbf{B} & \mathbf{0} \\ \mathbf{B} & \mathbf{D} & \mathbf{0} \\ \mathbf{0} & \mathbf{0} & \mathbf{A}^s \end{bmatrix} \quad (11)$$

where,

$$(A_{ij}, B_{ij}, D_{ij}) = \int_{-h/2}^{h/2} \bar{Q}_{ij}(1, z, z^2) dz, \quad A_{ij}^s = K \int_{-h/2}^{h/2} \bar{Q}_{ij} dz \quad (12)$$

where A_{ij} , B_{ij} and D_{ij} are valid for $i, j = 1, 2, 6$, and A_{ij}^s for $i, j = 4, 5$ according to the Voigt notation. K denotes the transverse shear correction coefficient. A value of $K = 5/6$ was used for the analyses.

2.2. Curvilinear stiffener

Consider a stiffener attached to a plate as shown in the figure below.

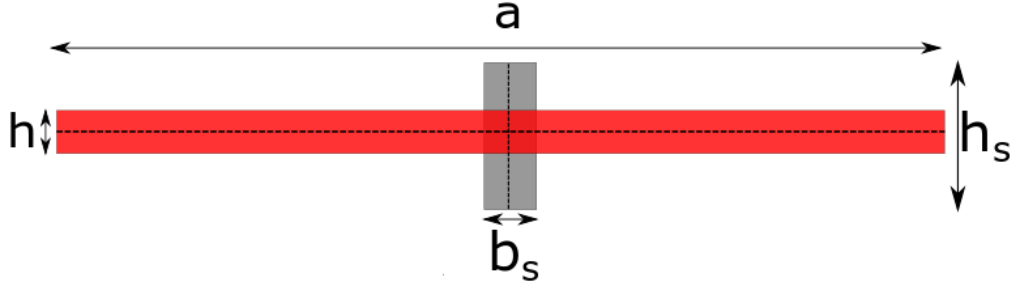


Figure 2: Composite plate (red) stiffened by a rectangular stiffener (gray)

The width and height of the rectangular stiffener are given as b_s and h_s , respectively. Details of the coordinate system and nomenclature can be found in [56]. The stiffener is modeled using 1D 2^{nd} order NURBS basis. The stiffener is modeled using the Timoshenko Beam theory. The modeling of stiffener for free vibration analysis follows the same procedure as Section 2.2. The stiffener strain energy U_s is written as:

$$U_s = \frac{1}{2} \int_{\Gamma} \varepsilon_s^{\mathbf{L}\mathbf{T}} \mathbf{D}_s \varepsilon_s^{\mathbf{L}} d\Gamma \quad (13)$$

The strain displacement relation of the composite stiffener is [57],

$$\varepsilon_s = \begin{Bmatrix} \varepsilon_t^0 \\ \gamma_n^0 \\ \gamma_b^0 \\ \kappa_t^0 \\ \kappa_n^0 \end{Bmatrix} = \begin{bmatrix} \frac{d}{dt} & \frac{1}{R} & 0 & 0 & 0 \\ -\frac{1}{R} & \frac{d}{dt} & 0 & 0 & 0 \\ 0 & 0 & \frac{d}{dt} & 1 & 0 \\ 0 & 0 & 0 & \frac{d}{dt} & \frac{1}{R} \\ 0 & 0 & 0 & -\frac{1}{R} & \frac{d}{dt} \end{bmatrix} \begin{Bmatrix} u_t \\ v_n \\ w_b \\ \beta_t \\ \beta_n \end{Bmatrix} = \mathbf{B}_s \mathbf{u}_s \quad (14)$$

where $\frac{1}{R}$ is the geometric curvature of the stiffener, computed at the integration points. Substituting Equation 14 into Equation 13 we get,

$$U_s = \frac{1}{2} \int_{\Gamma} \mathbf{u}_s^T \mathbf{B}_s^T \mathbf{D}_s \mathbf{B}_s \mathbf{u}_s d\Gamma, \quad (15)$$

The \mathbf{D}_s in the above strain energy equation is the rigidity matrix for the composite stiffener and is given by,

$$\begin{pmatrix} E_s A & 0 & 0 & E_s A e & 0 \\ 0 & G_s A_n & 0 & 0 & G_s A_n e \\ 0 & 0 & G_s A_b e & 0 & 0 \\ E_s A e & 0 & 0 & E_s I_n & 0 \\ 0 & G_s A_n e & 0 & 0 & G_s J_t \end{pmatrix} \quad (16)$$

The kinetic energy for the stiffener T_s is

$$T_s = \frac{1}{2} \int_{\Gamma} \dot{\mathbf{u}}_s^T m_s \dot{\mathbf{u}}_s d\Gamma \quad (17)$$

where m_s is the stiffener mass matrix and is given as,

$$m_s = \rho_s \begin{bmatrix} A & 0 & 0 & A e & 0 \\ 0 & A & 0 & 0 & A e \\ 0 & 0 & A & 0 & 0 \\ A e & 0 & 0 & I_n & 0 \\ 0 & A e & 0 & 0 & I_n + I_b \end{bmatrix} \quad (18)$$

Before building the linear system of equation of the stiffened plate, the degrees of freedom of the plate and curvilinear stiffener should be unified. Detailed steps to achieve this are as follows :

- First, the plate and the stiffener are meshed independently and the

location of the stiffener control points is identified. Take Figure 3 for instance, where the control point A belongs to the plate element k .

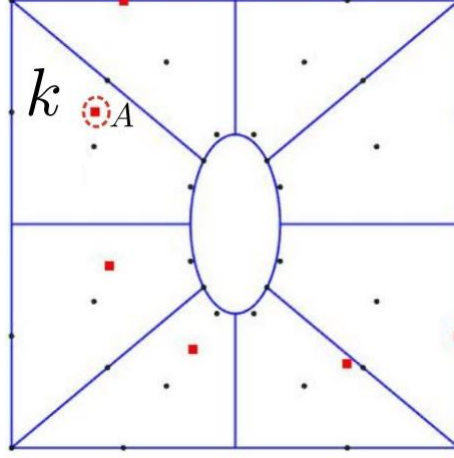


Figure 3: Mesh plot of the curvilinearly stiffened plate in the physical space.

We can compute the natural coordinates $(\bar{\xi}, \bar{\eta})$ of the stiffener control point in the plate element by solving Equation 19 since the stiffener and the plate control points are known.

$$\mathbf{r}_s|_A = \sum_{j=1}^4 R_j(\bar{\xi}_A, \bar{\eta}_A) \mathbf{x}_{p_j}|_k. \quad (19)$$

- Since the natural coordinates are not obtained, the displacement of the stiffener is:

$$\mathbf{u}_s|_A = \sum_{j=1}^4 R_j(\bar{\xi}_A, \bar{\eta}_A) \mathbf{u}_{p_j}|_k. \quad (20)$$

- The displacements of any points in the stiffener element can be expressed as:

$$\mathbf{u}_{sg} = \sum_{j=A} R_j(\varsigma) \mathbf{u}_{s_j}. \quad (21)$$

- Then, substituting Equation 20 into Equation 21 results in the following

equation:

$$\mathbf{u}_{sg} = \sum_{j=A} R_j(\varsigma) \sum_{i=1}^4 R_i(\bar{\xi}_j, \bar{\eta}_j) \mathbf{u}_{pi} |_k \quad (22)$$

- Rewriting the displacement approximations in a matrix form,

$$\mathbf{u}_{sg} = \mathbf{N}_{ps} \mathbf{u}_p |_k . \quad (23)$$

- Now the displacement \mathbf{u}_{sg} are described in the global coordinate system. Hence the stiffener displacements should be transformed to the local curvilinear coordinate system. The transformation matrix is:

$$\mathbf{T} = \begin{pmatrix} \cos \alpha & \sin \alpha & 0 & 0 & 0 \\ -\sin \alpha & \cos \alpha & 0 & 0 & 0 \\ 0 & 0 & 1 & 0 & 0 \\ 0 & 0 & 0 & \cos \alpha & \sin \alpha \\ 0 & 0 & 0 & -\sin \alpha & \cos \alpha \end{pmatrix}, \quad (24)$$

where α is the angle between the stiffener tangential direction t -axis and x -axis of the global coordinate system, whose value is calculated at each integration point.

$$\alpha = \tan^{-1} \left(\frac{y'}{x'} \right) \quad (25)$$

The prime ' denotes the first derivative with respect to the stiffener arc length, $d()/d\Gamma$.

Hence, the stiffener strain energy U_s and the kinetic energy T_s can be rewritten as,

$$U_s = \frac{1}{2} \int \mathbf{u}_p^T \mathbf{N}_{ps}^T \mathbf{T}^T \mathbf{B}_s^{LT} \mathbf{D}_s \mathbf{B}_s^L \mathbf{T} \mathbf{N}_{ps} \mathbf{u}_p d\Gamma, \quad (26)$$

$$T_s = \frac{1}{2} \int \dot{\mathbf{u}}_p^T \mathbf{N}_{ps}^T \mathbf{T}^T \mathbf{m}_s \mathbf{T} \mathbf{N}_{ps} \dot{\mathbf{u}}_p d\Gamma, \quad (27)$$

Hamilton's principle can now be used in deriving the weak form of the governing equation.

$$\int_{t_1}^{t_2} [(\delta U_p + \delta U_s) - (\delta T_p + \delta T_s)] dt = 0, \quad (28)$$

where t_1 and t_2 are the initial and final times, respectively. The principle expression is:

$$\int_{t_1}^{t_2} \left[\int_{\Omega} \delta \mathbf{u}_p^T (\mathbf{B}_p^{LT} \mathbf{D}_p \mathbf{B}_p^L) \mathbf{u}_p d\Omega + \int \delta \mathbf{u}_p^T (\mathbf{N}_{ps}^T \mathbf{T}^T \mathbf{B}_s^{LT} \mathbf{D}_s \mathbf{B}_s^L \mathbf{T} \mathbf{N}_{ps}) \mathbf{u}_p d\Gamma \right. \\ \left. - \int_{\Omega} \delta \mathbf{u}_p^T \mathbf{m}_p \ddot{\mathbf{u}}_p d\Omega - \int \delta \mathbf{u}_p^T (\mathbf{N}_{ps}^T \mathbf{T}^T \mathbf{m}_s \mathbf{T} \mathbf{N}_{ps}) \ddot{\mathbf{u}}_p d\Gamma \right] dt = 0. \quad (29)$$

To exhibit and substantiate the technique, free vibration analysis was conducted on multiple plates featuring diverse curvilinear stiffeners. The obtained outcomes were juxtaposed with established literature in certain instances, and in others, they were cross-referenced using widely recognized software such as ABAQUS. Through parametric investigations, the impact of both the cutout contour and the configuration and placement of the curvilinear stiffeners on the results was elucidated.

2.3. Modeling complicated cutouts using a single NURBS patch

In this case, first the inner and the outer profile of such a panel is constructed using 1D NURBS curves as shown in Figure 4. The control points and weights used to construct these curves are detailed in Table 1 and Table 2. Figure 5 and Table 3 describe the mesh and the connectivity matrix for the coarsest mesh respectively.

Table 1: Control points and weights of the inner curve

P_{ij}	x	6	5	4	3	2	2	2	2	2	1.414	4	4.243	6	5.657	8	5.657	6
	y	8	8	8	8	8	7	6	5	4	1.414	2	1.414	4	2.828	6	5.657	8
	z	0	0	0	0	0	0	0	0	0	0	0	0	0	0	0	0	0
W		1	1	1	1	1	1	1	1	1	0.707	1	0.707	1	0.707	1	0.707	1

Table 2: Control points and weights of the outer curve

P_{ij}	x	10	5	0	0	0	5	10	10	10
	y	10	10	10	5	0	0	0	5	10
	z	0	0	0	0	0	0	0	0	0
W		1	1	1	1	1	1	1	1	1

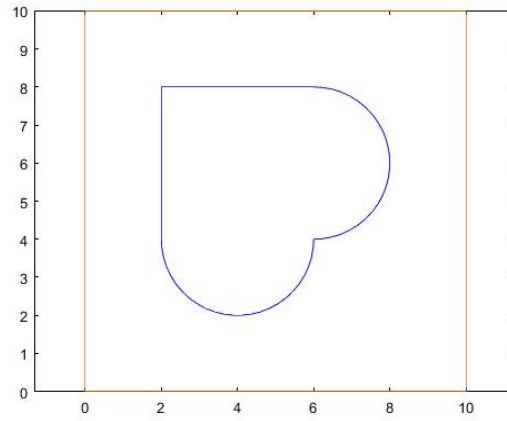
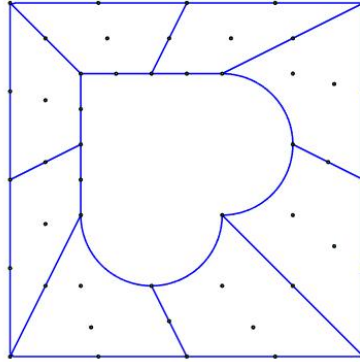
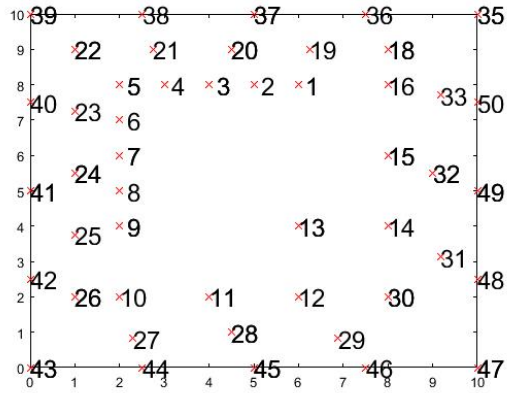


Figure 4: Inner and the outer curve to generate a plate with a complicated cutout



(a) Mesh Plot



(b) Connectivity Plot

Figure 5: Mesh and connectivity plot of a plate with a complicated cutout

Table 3: Connectivity matrix of a plate with a complicated cutout

Element	Node								
	1	2	3	4	5	6	7	8	9
1	1	2	3	18	19	20	35	36	37
2	3	4	5	20	21	22	37	38	39
3	5	6	7	22	23	24	39	40	41
4	7	8	9	24	25	26	41	42	43
5	9	10	11	26	27	28	43	44	45
6	11	12	13	28	29	30	45	46	47
7	13	14	15	30	31	32	47	48	49
8	15	16	1	32	33	18	49	50	35

2.4. A Three point parametrization of the curvilinear stiffener

Previous researchers [58], [56] and [59] involved curvilinear stiffeners with a parabolic profile. Using the parametric equation of the parabola and the start and the end point coordinates, one can obtain the three control points which could define the Bezier curve [60]. Since any parabolic stiffener can be represented using three control points, the coordinates of the end control points $\Delta\epsilon$ and Point 2 (where δ_{dist} refers to the point $[\delta_{dist}, \delta_{dist}]$) were used to represent the curvilinear stiffener.

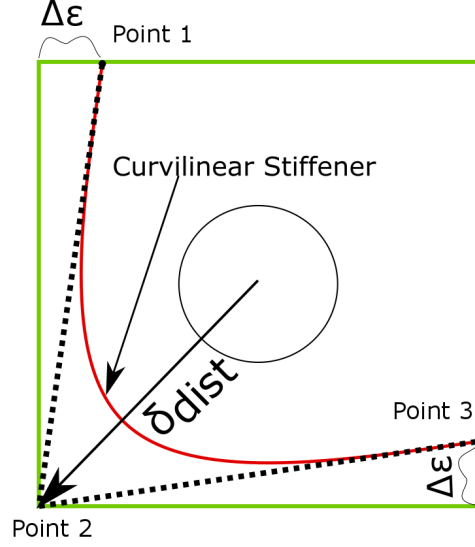


Figure 6: Parametrization of curvilinear stiffener

The FSDT which relies on C^0 continuity of the basis functions is employed in the patch interior unlike Kirchhoff-Love shell theory that relies on higher-order continuity of the basis functions as mentioned in [61].

3. Results and Discussion

To demonstrate and validate the method, free vibration analysis of several plates with different curvilinear stiffeners were carried out. Results are compared with existing literature for some cases while for some others, using commercially popular software like ABAQUS. Parametric studies were performed which show the influence of both the cutout profile and the shape and position of the curvilinear stiffeners in the results.

3.1. Isotropic plate with a circular hole at the center

In order to illustrate the performance of IGA code in modeling holes, an isotropic plate with a circular hole at the center was considered. The plate is assumed to have side length of 10 m and a thickness of 0.1 m. The hole has a radius of 1 m.

$$SSSS : \begin{cases} u_0 = v_0 = w_0 = \phi_y = \phi_z = 0 & \text{on } x = 0, a \\ u_0 = v_0 = w_0 = \phi_x = \phi_z = 0 & \text{on } y = 0, b \end{cases} \quad (30)$$

The material properties are :

$$E = 208 \text{ GPa}, \nu = 0.3, \rho = 8,000 \text{ kg/m}^2 \quad (31)$$

A normalized frequency parameter is defined by $\tilde{\omega} = [\rho h \omega^2 a^4 / D(1 - \nu^2)]^{1/4}$ with $D = Eh^3/12(1 - \nu^2)$.

Table 4: Normalized frequencies of clamped square plate with a circular hole.

Mode	Present	[62]	[41]
1	6.183	6.24	6.149
2	8.657	8.457	8.577
3	8.657	8.462	8.634
4	10.513	10.233	10.422
5	11.559	11.719	11.414
6	12.052	12.299	11.838
7	13.022	13.037	12.829
8	13.022	13.041	12.842

The first eight frequencies obtained by the current method are shown in Table 4. These results are compared against reference solutions in [62], [41]. The results are seen to be in good agreement with the reference solution.

3.2. Isotropic plate with a complicated cutout

The present method is applied to analyze an isotropic plate with a heart shaped cutout (Figure 4). The thickness of the plate is $h = 0.05\text{m}$ and the material parameters are

$$E = 200 \text{ GPa}, \nu = 0.3, \rho = 8000 \text{ kg/m}^3 \quad (32)$$

Shojaee et al. [63] analyzed the same geometry using IGA and classical laminate theory with multiple patches. The bending strip method was used to achieve compatibility between adjacent patches. In this work, the first order shear deformation theory was used and the plate was modeled with a single NURBS patch thus eliminating the use of multiple NURBS patches.

The normalized frequencies obtained using the present method are compared against some results from existing literature [63], MKI method [64], radial point interpolation method [65] and Element Free Galerkin method

Table 5: Normalized natural frequencies of a simply supported plate with a heart shaped complicated cutout.

Mode	MultiPatch	MKI	EFG	RIPM	ABAQUS	Present
1	5.193	5.39	5.453	4.919	4.948	4.945
2	6.579	7.502	8.069	6.398	6.426	6.441
3	6.597	8.347	9.554	6.775	6.796	6.804
4	7.819	10.636	10.099	8.613	8.616	8.585
5	8.812	11.048	11.328	9.016	9.020	9.031
6	9.42	12.894	12.765	10.738	10.720	10.670
7	10.742	13.71	13.685	10.93	10.966	10.908
8	10.776	14.062	14.305	11.601	11.686	11.661
9	11.919	16.649	15.721	12.903	12.901	12.833
10	13.2	17.364	17.079	13.283	13.238	13.185

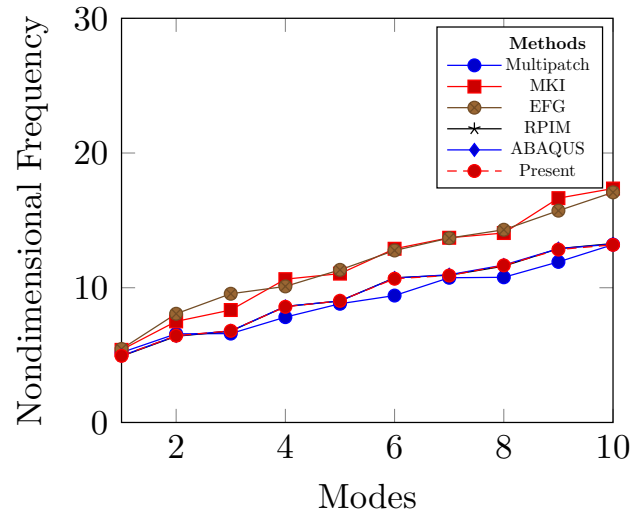


Figure 7: Normalized natural frequencies of a simply supported plate with a heart shaped complicated cutout.

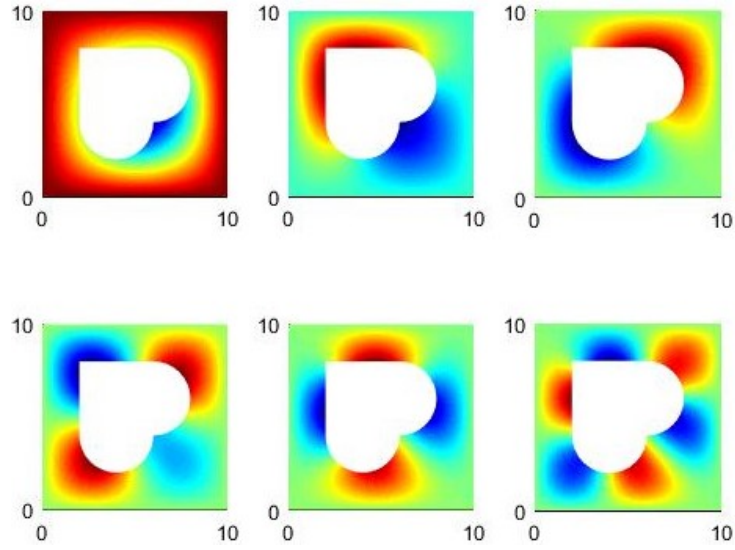


Figure 8: First six modes (IGA) of a simply supported square plate with a complicated cutout

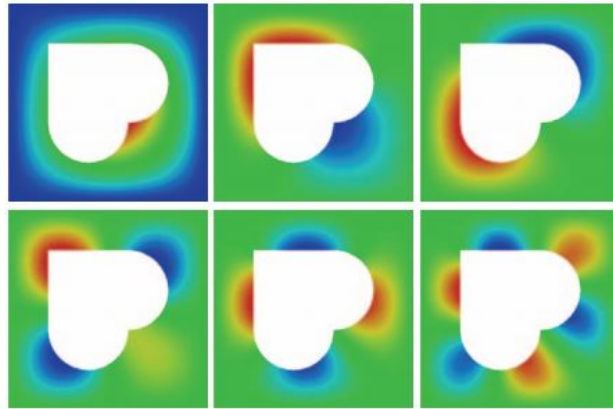


Figure 9: First six modes [63] of a simply supported plate with a heart shaped complicated cutout

[66]. The results can be seen in good agreement with the reference solutions for the simply supported boundary condition. As opposed to [63], the current method obviates the necessity to use the bending strip methods for patch coupling. The overall computational cost required is hence reduced significantly.

3.3. Vibration of a Composite plate with a heart shaped cutout

A three-layered symmetric crossply laminated composite plate is considered Figure 4. The ratio of elastic constants are as follows:

$$E_L/E_T = 2.45, G_{LT}/E_T = 0.48, G_{TT}/E_T = 0.2, \nu_{LT} = 0.23 \quad (33)$$

mass density = 8,000 kg/m^3 and thickness $h = 0.06m$. The frequency is normalized using $\tilde{\omega} = [\rho h \omega^2 a^4 / D_{0.1}]^{1/2}$, with $a=10m$ and $D_{0.1} = E_1 h^3 / 12(1 - \nu_{12}\nu_{21})$. The results were obtained for simply supported (SSSS) boundary condition.

$$SSSS : \begin{cases} u_0 = v_0 = w_0 = \phi_y = \phi_z = 0 & \text{on } x = 0, a \\ u_0 = v_0 = w_0 = \phi_x = \phi_z = 0 & \text{on } y = 0, b \end{cases} \quad (34)$$

The results were obtained for simply supported (SSSS) boundary conditions. The first six normalized frequencies of this model for various angle ply fiber orientations are presented in Table 6. The present solutions are compared with the results obtained by IGA and Kirchhoff theory with eight patches [63], EFG and MKI methods [64]. It can be observed that the present method delivers very good results which are in agreement with results from published literature for considered angle ply orientations.

Table 6: Normalized natural frequencies of a simply supported laminated plate with a heart shaped cutout for various angle ply orientations.

Angle ply	Method	Mode					
		1	2	3	4	5	6
(15°/-15°/15°)	Present	18.91	31.83	36.09	57.00	62.73	83.93
	8-patch IGA[63]	18.91	32.05	36.00	56.35	63.37	83.63
	EFG[64]	19.18	32.45	37.24	58.72	63.99	86.50
	MKI[64]	18.32	31.47	37.62	63.08	66.54	86.49
(30°/-30°/30°)	Present	20.40	33.66	37.23	59.20	65.03	87.92
	8-patch IGA[63]	20.32	33.93	37.07	58.48	65.90	87.97
	EFG[64]	20.93	34.92	39.10	62.22	67.05	92.72
	MKI[64]	20.31	33.99	39.90	58.11	69.70	92.10
(45°/-45°/45°)	Present	21.10	34.45	37.91	60.29	66.22	90.68
	8-patch IGA[63]	20.98	34.85	37.56	59.33	67.52	91.22
	EFG[64]	21.74	36.08	39.98	63.90	68.53	96.77
	MKI[64]	20.99	34.90	39.27	63.38	69.02	96.59

3.4. Curvilinearly stiffened composite panels with central circular cutout

In this section, the influence of central cutouts on clamped stiffened composite panels is studied.

$$\text{Clamped} : u_0 = 0, v_0 = 0, \psi_x = 0, \psi_y = 0, w_0 = 0 \quad (35)$$

on all four edges. The stiffener is assumed to be fabricated from isotropic material with Young's modulus = E_T , Poisson's ratio = ν_{LT} and coefficient of thermal expansion = α_0 . The stiffness ratio $\gamma = EI/bD$ and the area ratio $\delta = A_s/bt_p$ are 5 and 0.1 respectively, unless specified otherwise. The ratio of elastic constants are as follows:

$$E_L/E_T = 15, G_{LT}/E_T = 0.5, G_{TT}/E_T = 0.3356, \nu_{LT} = 0.3 \quad (36)$$

mass density = 8,000 kg/m³ and thickness $h = 0.01$ m. The frequency is normalized using

$$\tilde{\omega} = [\rho h \omega^2 a^4 / D_{0.1}]^{1/2} \quad (37)$$

with $a=1$ m and $D_{0.1} = E_1 h^3 / 12(1 - \nu_{12}\nu_{21})$. To check the accuracy of the displacement compatibility algorithm, results for clamped curvilinearly stiffened composite plate are compared with those obtained using ABAQUS. The

curvilinear stiffener configuration was adopted from [67] and scaled proportionally to match the dimensions of the plate. From the ABAQUS library, the plate was meshed using 2040 S8R elements and curvilinear stiffener was meshed using 192 elements S8R elements (48 divisions along the arc length and 4 divisions along the depth direction). The IGA plate model was meshed using 1024 elements and the curvilinear stiffener using 32 elements. The normalized fundamental frequency was observed to converge for these mesh configurations. The first five eigenmodes were extracted for this case. The eigenmode plots obtained using the IGA approach are similar to the ones obtained using ABAQUS as can be seen from Figure 10.

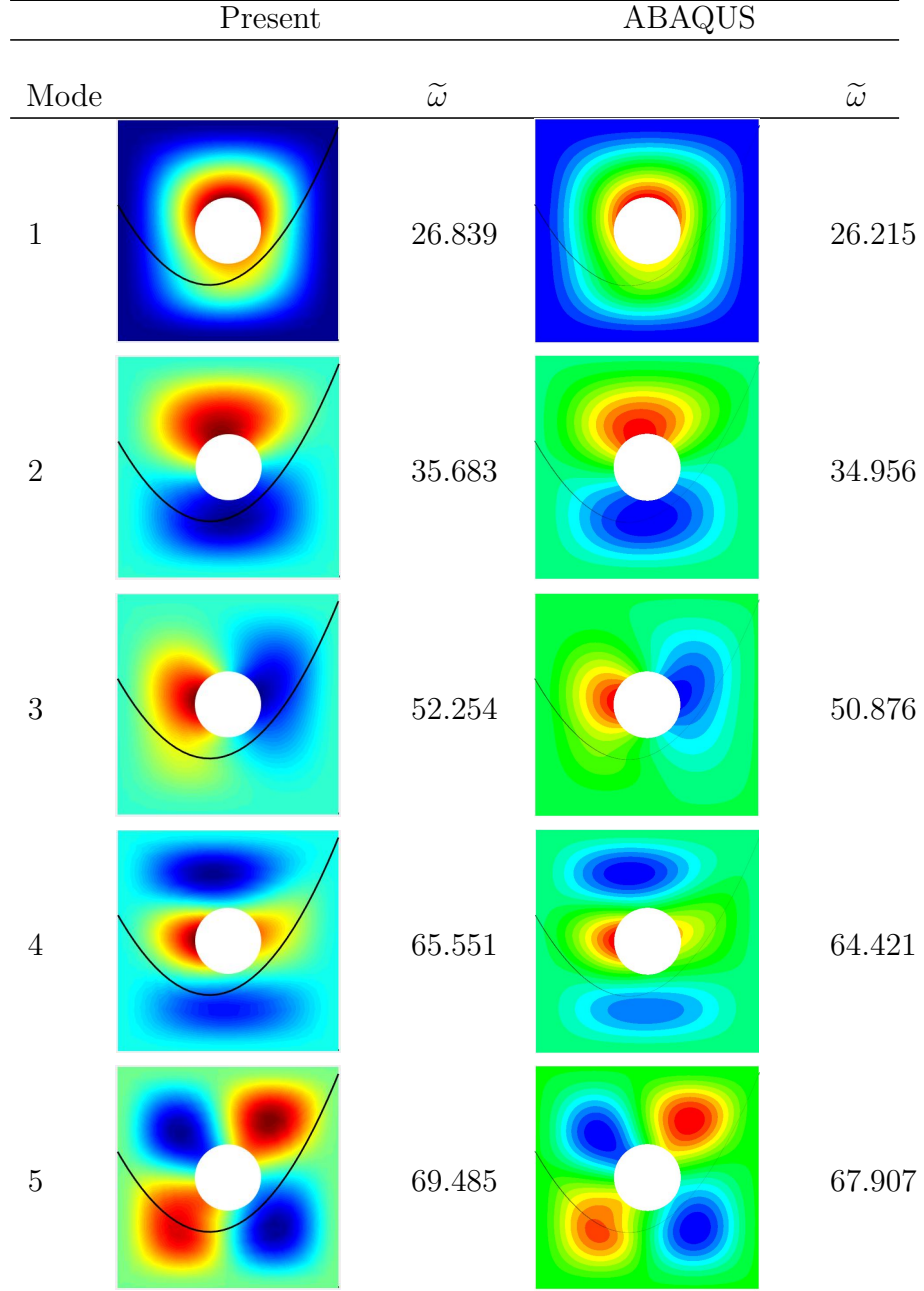


Figure 10: The first five eigenmode shape plots for a plate with curvilinear stiffener using a IGA and ABAQUS, a commercial available software.

3.5. Curvilinearly stiffened composite panels with an elliptical central cutout

In this section, results of curvilinearly stiffened composite panels with elliptical cutouts are presented. The ratio of elastic constants are as follows:

$$E_L/E_T = 15, G_{LT}/E_T = 0.5, G_{TT}/E_T = 0.3356, \nu_{LT} = 0.3 \quad (38)$$

mass density = 8,000 kg/m^3 and thickness $h = 0.01$ m . The frequency is normalized by $\tilde{\omega} = [\rho h \omega^2 a^4 / D_{0.1}]^{1/2}$, with $a=1$ m and $D_{0.1} = E_1 h^3 / 12(1 - \nu_{12}\nu_{21})$. The results were obtained for clamped boundary condition.

An ellipse of semi-major axis = 0.2 m and semi-minor axis = 0.1 m is considered for all cases. The normalized first ten frequencies of a stiffend four layer composite laminate plate with respect to ply orientations, stiffness ratios and different stiffener profiles (defined by $\Delta\epsilon$ Figure 6) are presented in Table 8 and Table 9 and their fifth mode shapes are shown in Figures 8, 9, 10, 11, 12 and 14.

Table 8: Normalized frequencies for different ply orientations for $\gamma = 5$ and $\Delta\epsilon = 0$

Mode	Antisymmetric Crossply	Symmetric Crossply	Symmetric Angleply	Antisymmetric Angleply
1	23.986	25.407	23.572	23.582
2	38.356	34.523	37.198	38.044
3	44.347	47.911	39.978	42.451
4	61.730	60.599	60.905	64.111
5	76.728	64.747	71.808	73.009
6	84.472	77.037	80.460	76.987
7	92.642	88.814	86.570	83.375
8	97.597	100.505	88.596	100.486
9	113.239	112.436	106.260	110.241
10	131.673	117.184	114.723	115.131

Table 9: Normalized frequencies for different ply orientations for $\gamma = 5$ and $\Delta\epsilon = 0.25$

Mode	Antisymmetric Crossply	Symmetric Crossply	Symmetric Angleply	Antisymmetric Angleply
1	25.733	26.909	24.646	25.235
2	37.732	35.836	36.676	37.132
3	48.315	49.624	43.724	47.161
4	69.413	61.422	68.170	69.795
5	74.287	73.238	70.369	70.890
6	90.708	85.848	87.059	84.483
7	97.896	94.369	92.601	91.590
8	112.175	106.567	100.993	110.461
9	116.899	120.171	109.681	112.065
10	134.109	126.330	116.890	124.329

Table 10: Normalized frequencies for different ply orientations for $\gamma = 10$ and $\Delta\epsilon = 0$

Mode	Antisymmetric Crossply	Symmetric Crossply	Symmetric Angleply	Antisymmetric Angleply
1	24.558	25.884	24.338	24.204
2	39.728	35.893	38.942	39.532
3	44.829	48.349	40.774	42.883
4	63.772	62.179	62.164	65.975
5	78.058	66.348	73.699	74.667
6	86.129	79.246	81.491	77.525
7	92.842	89.915	87.746	83.964
8	99.651	100.505	88.801	101.741
9	114.029	112.995	108.705	111.953
10	134.182	119.439	115.836	118.263

Table 11: Normalized frequencies for different ply orientations for $\gamma = 10$ and $\Delta\epsilon = 0.25$

Mode	Antisymmetric Crossply	Symmetric Crossply	Symmetric Angleply	Antisymmetric Angleply
1	27.711	28.829	26.494	27.386
2	39.709	38.489	38.548	38.691
3	52.994	51.992	48.197	52.150
4	74.603	65.702	71.611	72.942
5	77.687	79.184	76.178	74.211
6	93.429	89.734	89.045	87.193
7	102.543	98.080	95.125	99.094
8	115.133	111.041	107.583	113.098
9	126.002	121.882	113.833	114.182
10	137.331	133.214	124.795	139.792

Table 12: The fifth mode shape plots for different ply orientations for $\gamma = 5$ and $\Delta\epsilon = 0$

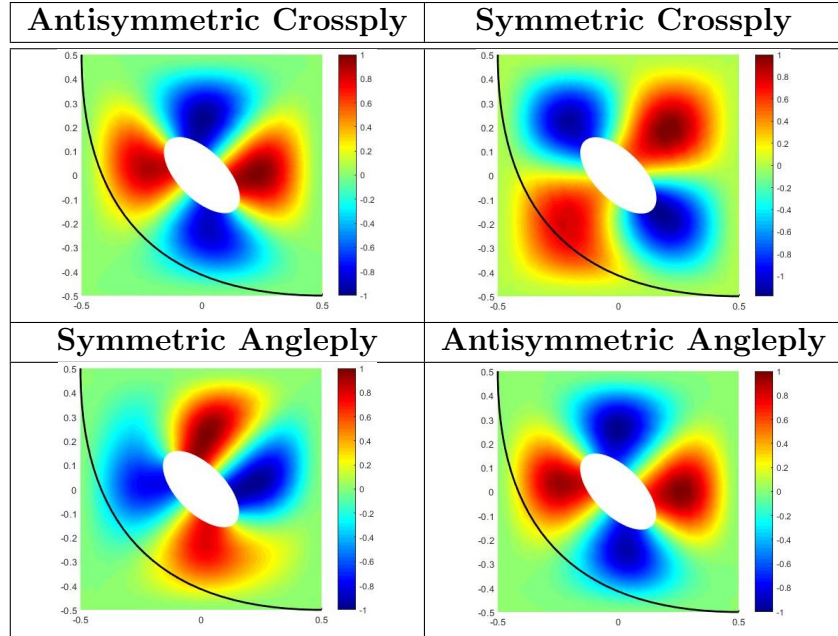


Table 13: The fifth mode shape plots for different ply orientations for $\gamma = 5$ and $\Delta\epsilon = 0.25$

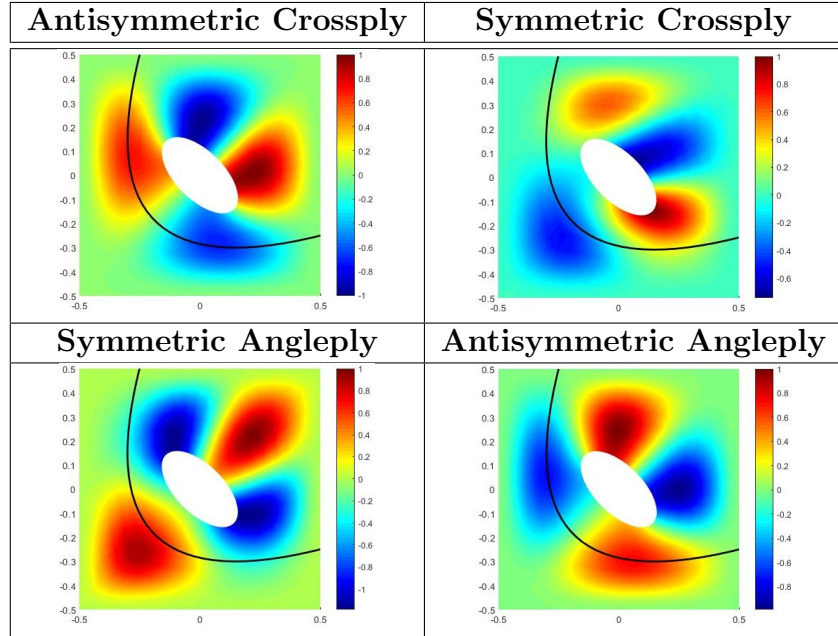


Table 14: The fifth mode shape plots for different ply orientations for $\gamma = 10$ and $\Delta\epsilon = 0$

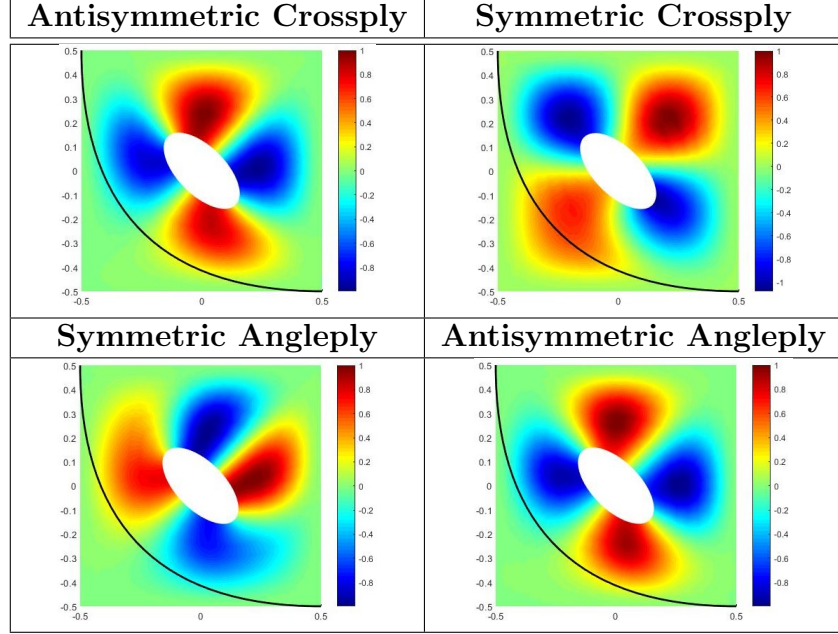
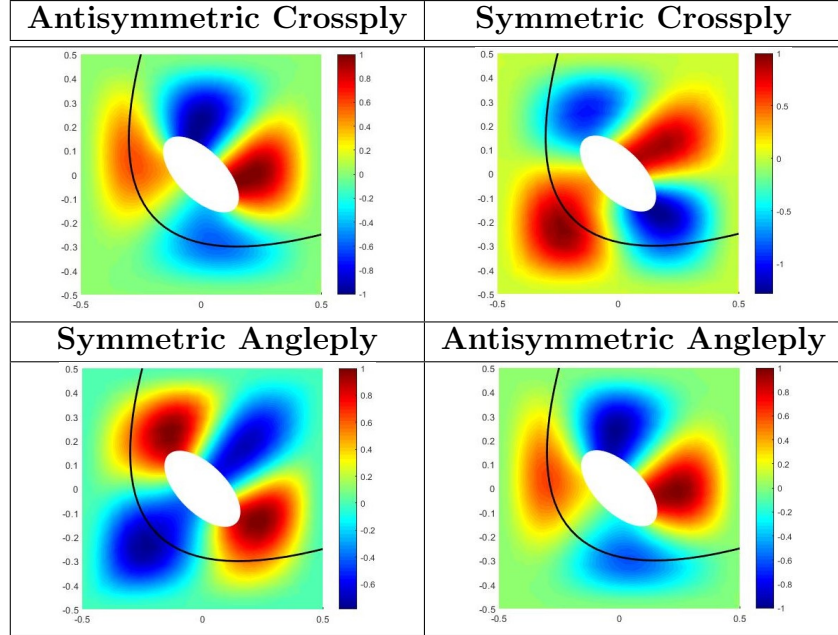


Table 15: The fifth mode shape plots for different ply orientations for $\gamma = 10$ and $\Delta\epsilon = 0.25$



This section discusses the vibration analysis of curvilinearly stiffened plate with cutouts using a single NURBS patch. The efficiency of this method is described using numerical examples of laminated plates containing cutouts of various shapes and dimensions and for different boundary conditions, stiffener locations and curvature.

4. Conclusions

The application of the isogeometric technique has proven effective in conducting vibration analysis on a curvilinearly stiffened plate containing cutouts. This was achieved by employing a sole NURBS patch. The method's effectiveness is demonstrated through numerical instances involving intricate cutout designs of various sizes and shapes, alongside diverse boundary conditions, locations of stiffeners, and curvatures for stiffened laminated plates. The utilization of a single NURBS patch to represent complex cutout shapes showcases impressive conformity between the outcomes obtained and those generated by contemporary methodologies. The isogeometric analysis a computationally efficient method that could be used along with powerful optimization algorithms like Particle Swarm Optimization and Differential Evolution [68] to perform structural optimization and come up with light-weight designs.

References

- [1] W. J. Renton, D. Olcott, W. Roeseler, R. Batzer, W. Baron, and A. Velicki, "Future of Flight Vehicle Structures (2000 to 2023)," *Journal of Aircraft*, vol. 41, no. 5, pp. 986–998, 2004.
- [2] S. De, K. Singh, J. Seo, R. K. Kapania, E. Ostergaard, N. Angelini, and R. Aguero, "Structural design and optimization of commercial vehicles chassis under multiple load cases and constraints," in *AIAA Scitech 2019 Forum*, 2019, p. 0705.
- [3] M. Jrad, S. De, and R. K. Kapania, "Global-local aeroelastic optimization of internal structure of transport aircraft wing," in *18th AIAA/ISSMO Multidisciplinary Analysis and Optimization Conference*, 2017, p. 4321.

- [4] J. H. Robinson, S. Doyle, G. Ogawa, M. Baker, S. De, M. Jrad, and R. K. Kapania, “Aeroelastic optimization of wing structure using curvilinear spars and ribs (sparibs),” in *17th AIAA/ISSMO Multidisciplinary Analysis and Optimization Conference*, 2016, p. 3994.
- [5] S. De, K. Singh, J. Seo, R. K. Kapania, E. Ostergaard, N. Angelini, and R. Agüero, “Lightweight chassis design of hybrid trucks considering multiple road conditions and constraints,” *World Electric Vehicle Journal*, vol. 12, no. 1, p. 3, 2021.
- [6] S. De, M. Jrad, D. Locatelli, R. K. Kapania, and M. Baker, “Sparibs geometry parameterization for wings with multiple sections using single design space,” in *58th AIAA/ASCE/AHS/ASC Structures, Structural Dynamics, and Materials Conference*, 2017, p. 0570.
- [7] S. De, K. Singh, J. Seo, R. Kapania, R. Agüero, E. Ostergaard, and N. Angelini, “Unconventional truck chassis design with multi-functional cross members,” SAE Technical Paper, Tech. Rep., 2019.
- [8] S. De, “Structural modeling and optimization of aircraft wings having curvilinear spars and ribs (sparibs),” Ph.D. dissertation, Virginia Tech, 2017.
- [9] S. De, K. Singh, B. Alanbay, R. K. Kapania, and R. Agüero, “Structural optimization of truck front-frame under multiple load cases,” in *ASME International Mechanical Engineering Congress and Exposition*, vol. 52187. American Society of Mechanical Engineers, 2018, p. V013T05A039.
- [10] S. De and R. K. Kapania, “Algorithms for 2d mesh decomposition in distributed design optimization,” *arXiv preprint arXiv:2002.00525*, 2020.
- [11] S. De, “Manual of ebf3glwingopt.”
- [12] R. K. Kapania, M. Jrad, and S. De, “Manual of ebf3glwingopt.”
- [13] Y. Zhang and C. Yang, “Recent developments in finite element analysis for laminated composite plates,” *Composite Structures*, vol. 88, no. 1, pp. 147–157, 2009.

- [14] J. Reddy and A. Khdeir, “Buckling and vibration of laminated composite plates using various plate theories,” *AIAA Journal*, vol. 27, no. 12, pp. 1808–1817, 1989.
- [15] E. Carrera, P. Nali, S. Lecca, and M. Soave, “Effects of in-plane loading on vibration of composite plates,” *Shock and Vibration*, vol. 19, no. 4, pp. 619–634, 2012.
- [16] D.-M. Lee and I. Lee, “Vibration analysis of anisotropic plates with eccentric stiffeners,” *Computers & structures*, vol. 57, no. 1, pp. 99–105, 1995.
- [17] R. Rikards, A. Chate, and O. Ozolinsh, “Analysis for buckling and vibrations of composite stiffened shells and plates,” *Composite Structures*, vol. 51, no. 4, pp. 361–370, 2001.
- [18] S. Patel, P. Datta, and A. H. Sheikh, “Buckling and dynamic instability analysis of stiffened shell panels,” *Thin-Walled Structures*, vol. 44, no. 3, pp. 321–333, 2006.
- [19] M. Mukhopadhyay and A. Mukherjee, “Finite element buckling analysis of stiffened plates,” *Computers & structures*, vol. 34, no. 6, pp. 795–803, 1990.
- [20] Y. S. Kumar and M. Mukhopadhyay, “A new triangular stiffened plate element for laminate analysis,” *Composites Science and Technology*, vol. 60, no. 6, pp. 935–943, 2000.
- [21] P. Shi, R. K. Kapania, and C. Dong, “Vibration and buckling analysis of curvilinearly stiffened plates using finite element method,” *AIAA Journal*, vol. 53, no. 5, pp. 1319–1335, 2015.
- [22] B. G. Prusty and S. K. Satsangi, “Finite element transient dynamic analysis of laminated stiffened shells,” *Journal of Sound and Vibration*, vol. 248, no. 2, pp. 215–233, 2001.
- [23] T. J. Hughes, J. A. Cottrell, and Y. Bazilevs, “Isogeometric analysis: CAD, finite elements, NURBS, exact geometry and mesh refinement,” *Computer Methods in Applied Mechanics and Engineering*, vol. 194, no. 39-41, pp. 4135–4195, 2005.

- [24] Austin Cottrell, J.; Hughes, T.J.R.; Bazilevs, Y., *Isogeometric Analysis: Toward Integration of CAD and FEA*. John Wiley & Sons, 2009.
- [25] J. A. Cottrell, A. Reali, Y. Bazilevs, and T. J. Hughes, “Isogeometric analysis of structural vibrations,” *Computer methods in Applied Mechanics and Engineering*, vol. 195, no. 41-43, pp. 5257–5296, 2006.
- [26] N. D. Manh, A. Evgrafov, A. R. Gersborg, and J. Gravesen, “Isogeometric shape optimization of vibrating membranes,” *Computer Methods in Applied Mechanics and Engineering*, vol. 200, no. 13-16, pp. 1343–1353, 2011.
- [27] Y. Bazilevs, M.-C. Hsu, and M. Scott, “Isogeometric fluid–structure interaction analysis with emphasis on non-matching discretizations, and with application to wind turbines,” *Computer Methods in Applied Mechanics and Engineering*, vol. 249, pp. 28–41, 2012.
- [28] N. Nguyen-Thanh, N. Valizadeh, M. Nguyen, H. Nguyen-Xuan, X. Zhuang, P. Areias, G. Zi, Y. Bazilevs, L. De Lorenzis, and T. Rabczuk, “An extended isogeometric thin shell analysis based on Kirchhoff–Love theory,” *Computer Methods in Applied Mechanics and Engineering*, vol. 284, pp. 265–291, 2015.
- [29] L. V. Tran, H. A. Ly, J. Lee, M. A. Wahab, and H. Nguyen-Xuan, “Vibration analysis of cracked FGM plates using higher-order shear deformation theory and extended isogeometric approach,” *International Journal of Mechanical Sciences*, vol. 96, pp. 65–78, 2015.
- [30] H. Kapoor and R. K. Kapania, “Geometrically nonlinear NURBS isogeometric finite element analysis of laminated composite plates,” *Composite Structures*, vol. 94, no. 12, pp. 3434–3447, 2012.
- [31] H. Kapoor, R. K. Kapania, and S. R. Soni, “Interlaminar stress calculation in composite and sandwich plates in NURBS Isogeometric finite element analysis,” *Composite Structures*, vol. 106, pp. 537–548, 2013.
- [32] L. V. Tran, C. H. Thai, H. T. Le, B. S. Gan, and J. Lee, “Engineering Analysis with Boundary Elements Isogeometric analysis of laminated composite plates based on a four-variable refined plate theory,” *Engineering Analysis with Boundary Elements*, vol. 47, pp. 68–81, 2014.

- [33] L. V. Tran, A. J. Ferreira, and H. Nguyen-Xuan, “Isogeometric analysis of functionally graded plates using higher-order shear deformation theory,” *Composites Part B: Engineering*, vol. 51, pp. 368–383, 2013.
- [34] P. Phung-Van, L. V. Tran, A. Ferreira, H. Nguyen-Xuan, and M. Abdel-Wahab, “Nonlinear transient isogeometric analysis of smart piezoelectric functionally graded material plates based on generalized shear deformation theory under thermo-electro-mechanical loads,” *Nonlinear Dynamics*, vol. 87, no. 2, pp. 879–894, 2017.
- [35] E. Carrera, “Transverse Normal Strain Effect on Thermal Stress Analysis of Homogeneous and Layered Plates,” *AIAA Journal*, vol. 43, no. 10, pp. 2232–2242, 2005.
- [36] X. Qin, C. Dong, F. Wang, and Y. Gong, “Free vibration analysis of isogeometric curvilinearly stiffened shells,” *Thin-Walled Structures*, vol. 116, pp. 124–135, 2017.
- [37] G. Eccher, K. J. R. Rasmussen, and R. Zandonini, “Elastic buckling analysis of perforated thin-walled structures by the isoparametric spline finite strip method,” *Thin-Walled Structures*, vol. 46, no. 2, pp. 165–191, 2008.
- [38] G. B. Chai, “Free vibration of laminated composite plates with a central circular hole,” *Composite Structures*, vol. 35, no. 4, pp. 357–368, 1996.
- [39] M. Aydin Komur, F. Sen, A. Atas, and N. Arslan, “Buckling analysis of laminated composite plates with an elliptical/circular cutout using FEM,” *Advances in Engineering Software*, vol. 41, no. 2, pp. 161–164, 2010.
- [40] D. Kumar and S. B. Singh, “Effects of boundary conditions on buckling and postbuckling responses of composite laminate with various shaped cutouts,” *Composite Structures*, vol. 92, no. 3, pp. 769–779, 2010.
- [41] G. R. Liu, X. Zhao, K. Y. Dai, Z. H. Zhong, G. Y. Li, and X. Han, “Static and free vibration analysis of laminated composite plates using the conforming radial point interpolation method,” *Composites Science and Technology*, vol. 68, no. 2, pp. 354–366, 2008.

- [42] C. C. Chen, S. Kitipornchai, C. W. Lim, and K. M. Liew, “Free vibration of symmetrically laminated thick-perforated plates,” *Journal of Sound and Vibration*, vol. 230, no. 1, pp. 111–132, 2000.
- [43] H. R. Ovesy and J. Fazilati, “Buckling and free vibration finite strip analysis of composite plates with cutout based on two different modeling approaches,” *Composite Structures*, vol. 94, no. 3, pp. 1250–1258, 2012.
- [44] S. Natarajan, A. J. Ferreira, and H. Nguyen-Xuan, “Analysis of cross-ply laminated plates using isogeometric analysis and unified formulation,” *Curved and Layered Structures*, vol. 1, no. 1, pp. 1–10, 2014.
- [45] T. T. Yu, S. Yin, T. Q. Bui, and S. Hirose, “A simple FSDT-based isogeometric analysis for geometrically nonlinear analysis of functionally graded plates,” *Finite Elements in Analysis and Design*, vol. 96, no. C, pp. 1–10, 2015.
- [46] Y. Bazilevs, C. Michler, V. M. Calo, and T. J. Hughes, “Isogeometric variational multiscale modeling of wall-bounded turbulent flows with weakly enforced boundary conditions on unstretched meshes,” *Computer Methods in Applied Mechanics and Engineering*, vol. 199, no. 13-16, pp. 780–790, 2010.
- [47] Y. Bazilevs, V. M. Calo, T. J. R. Hughes, and Y. Zhang, “Isogeometric fluid-structure interaction: theory, algorithms, and computations,” *Computational Mechanics*, vol. 43, no. 1, pp. 3–37, 2008.
- [48] J. A. Evans, Y. Bazilevs, I. Babuška, and T. J. Hughes, “ n -Widths, sup -infs, and optimality ratios for the k -version of the isogeometric finite element method,” *Computer Methods in Applied Mechanics and Engineering*, vol. 198, no. 21-26, pp. 1726–1741, 2009.
- [49] T. J. R. Hughes, A. Reali, and G. Sangalli, “Efficient quadrature for NURBS-based isogeometric analysis,” *Computer Methods in Applied Mechanics and Engineering*, vol. 199, no. 5-8, pp. 301–313, 2010.
- [50] F. Auricchio, F. Calabrò, T. J. Hughes, A. Reali, and G. Sangalli, “A simple algorithm for obtaining nearly optimal quadrature rules for NURBS-based isogeometric analysis,” *Computer Methods in Applied Mechanics and Engineering*, vol. 249-252, pp. 15–27, 2012.

- [51] N. Valizadeh, T. Bui, V. Vu, H. Thai, and M. Nguyen, “Isogeometric Simulation for Buckling, Free and Forced Vibration of Orthotropic Plates,” *International Journal of Applied Mechanics*, vol. 05, no. 02, p. 1350017, 2013.
- [52] S. Yin, J. S. Hale, T. Yu, T. Q. Bui, and S. P. Bordas, “Isogeometric locking-free plate element: A simple first order shear deformation theory for functionally graded plates,” *Composite Structures*, vol. 118, no. 1, pp. 121–138, 2014.
- [53] C. V. Verhoosel, M. A. Scott, T. J. R. Hughes, and R. de Borst, “An isogeometric analysis approach to gradient damage models,” *International Journal for Numerical Methods in Engineering*, vol. 86, no. 1, pp. 115–134, 2011.
- [54] J. Lu, “Isogeometric contact analysis: Geometric basis and formulation for frictionless contact,” *Computer Methods in Applied Mechanics and Engineering*, vol. 200, no. 5-8, pp. 726–741, 2011.
- [55] W. A. Wall, M. A. Frenzel, and C. Cyron, “Isogeometric structural shape optimization,” *Computer Methods in Applied Mechanics and Engineering*, vol. 197, no. 33-40, pp. 2976–2988, 2008.
- [56] W. Zhao and R. K. Kapania, “Buckling analysis of unitized curvilinearly stiffened composite panels,” *Composite Structures*, vol. 135, pp. 365–382, 2016.
- [57] L. Martini and R. Vitaliani, “On the polynomial convergent formulation of a C^0 isoparametric skew beam element,” *Computers and Structures*, vol. 29, no. 3, pp. 437–449, 1988.
- [58] A. Y. Tamijani and R. K. Kapania, “Buckling and Static Analysis of Curvilinearly Stiffened Plates Using Mesh-Free Method,” *AIAA Journal*, vol. 48, no. 12, pp. 2739–2751, Dec 2010.
- [59] P. Shi, R. K. Kapania, and C. Y. Dong, “Vibration and Buckling Analysis of Curvilinearly Stiffened Plates Using Finite Element Method,” *AIAA Journal*, vol. 53, no. 5, pp. 1319–1335, 2015.
- [60] L. L. Piegl and W. Tiller, *The NURBS Book*. Springer Science & Business Media, 1996, vol. 28.

- [61] Y. Bazilevs, V. M. Calo, J. A. Cottrell, J. A. Evans, T. J. Hughes, S. Lipton, M. A. Scott, and T. W. Sederberg, “Isogeometric analysis using T-splines,” *Computer Methods in Applied Mechanics and Engineering*, vol. 199, no. 5-8, pp. 229–263, 2010.
- [62] M. Huang and T. Sakiyama, “Free vibration analysis of rectangular plates with variously-shaped holes,” *Journal of Sound and Vibration*, vol. 226, no. 4, pp. 769–786, 1999.
- [63] S. Shojaee, E. Izadpanah, N. Valizadeh, and J. Kiendl, “Free vibration analysis of thin plates by using a NURBS-based isogeometric approach,” *Finite Elements in Analysis and Design*, vol. 61, pp. 23–34, 2012.
- [64] T. Q. Bui, M. N. Nguyen, and C. Zhang, “An efficient meshfree method for vibration analysis of laminated composite plates,” *Computational Mechanics*, vol. 48, no. 2, pp. 175–193, 2011.
- [65] X. Cui, G. Liu, G. Li, and G. Zhang, “A thin plate formulation without rotation dofs based on the radial point interpolation method and triangular cells,” *International journal for numerical methods in engineering*, vol. 85, no. 8, pp. 958–986, 2011.
- [66] G. R. Liu and X. L. Chen, “A mesh-free method for static and free vibration analyses of thin plates of complicated shape,” *Journal of Sound and Vibration*, vol. 241, no. 5, pp. 839–855, 2001.
- [67] A. Y. Tamijani and R. K. Kapania, “Buckling and static analysis of curvilinearly stiffened plates using mesh-free method,” *AIAA Journal*, vol. 48, no. 12, pp. 2739–2751, 2010.
- [68] S. Biswas, D. Saha, S. De, A. D. Cobb, S. Das, and B. A. Jalaian, “Improving differential evolution through bayesian hyperparameter optimization,” in *2021 IEEE Congress on evolutionary computation (CEC)*. IEEE, 2021, pp. 832–840.